Characterization of the Electronic Structure in High-Hole Mobility SnO Film

Actual knowledge of the intrinsic electronic characteristics of p-type oxide semiconductors should help guide the design of innovative electronic devices. The electronic characteristics of oxide semiconductors in the thin-film form potentially differ from those in the bulk form owing to lattice strain. Here, we report on the empirical band structure of SnO film having a higher hole mobility than the theoretically expected values for bulk SnO. Angle-resolved photoemission spectroscopy measurements revealed that the uppermost valence band is more dispersive than the theoretical predictions. Our findings unveil the underlying mechanism of the semiconductor properties of SnO films.

The characteristic orbital hybridization between anions and ns^2 cations provides some fascinating properties for realizing innovative electronic devices. Recently, many appealing oxide semiconductors based on this hybridization have been systematically predicted by high-throughput computational screening [1]. Based on the identification, several ns^2 cations such as Sn^{2+} or Bi^{3+} based oxides have been developed as p-type oxide semiconductors [2-6]. The crucial design concept of these materials is the delocalization of holes in their valence band maximum (VBM) by the isotropic and broad cation orbital, which results in dispersive band edges. In order to prove this design concept, it is necessary to observe the dispersive valence band edges experimentally and compare them with theoretical predictions.

Herein, we unveil the empirical band structure of SnO film through angle-resolved photoemission spectroscopy (ARPES) measurements. SnO is a well-known prototype material of the above state-of-the-art p-type oxide semiconductors. Moreover, the hole mobility (μ_{hole}) of SnO films has been greatly improved through precise control of the growth conditions [7]. The observed high μ_{hole} for the thin-film form is higher than the theoretically expected value for the bulk form [8]. This suggests that correct and precise elucidation of the actual electronic structure in the thin-film form (not bulk) is crucial for designing practical thin-film devices.

Figures 1a and b display a summary of the ARPES intensity plots with two different polarizations of incident light along the Γ–X–Γ and Γ–M–Γ lines, respectively. The uppermost valence band is clearly observed for linear-horizontal (LH) polarization but hardly observed for linear-vertical (LV) polarization. Based on dipole transition selection rules for optical transitions [9], the photoelectrons are only detected when the initial state is symmetric and antisymmetric, with respect to the symmetry operation, to the detection plane for LH and LV polarizations, respectively. Because the point group along the symmetric Γ–X (Γ–M) line is C_{2v}, the bands with Γ_1 and Γ_2 (Γ_1 and Γ_4) symmetries should be observed for LH polarization, whereas the bands with Γ_3 and Γ_4 (Γ_2 and Γ_3) symmetries should be observed for LV polarization. According to our calculations the uppermost valence band exhibits Γ_2 and Γ_4 symmetry along the Γ–X and Γ–M lines, respectively; therefore, the observed polarization dichroism must be caused by the dipole selection rule. Our calculation suggests that the uppermost valence band near E_F, that is, the VBM, mainly originates from the Sn 5*s* and O 2p_z orbitals, which are symmetric with respect to the detection plane.

Overall, the dispersion shapes and the polarization properties of all bands can be *qualitatively* explained by our calculation. However, a closer observation reveals that the bandwidth of the uppermost valence band is broader than that predicted through the calculation, and the other valence bands are pushed down to the higher binding energy side. The increase in curvature near the VBM suggests a higher μ_{hole} owing to the decrease in the effective mass compared to that expected through the calculations for the bulk form. Previous calculations indicated anti-bonding Sn-O and Sn-Sn character for the uppermost valence band [10, 11]. Therefore, the observed broadening in the thin-film form could be caused by the enhancement of hybridization between Sn 5*s*, 5*p*, and O 2*p* orbitals potentially owing to the changes in the crystal structure triggered by the lattice strain [12, 13].

In order to elucidate the possible changes in the crystal structure, we focused on the long- and short-term crystal structure of SnO film investigated using X-ray diffraction and X-ray absorption spectroscopy (XAS). The observed Bragg peaks of the SnO film showed shrinkage and expansion of the out-of-plane and in-plane lattice constant, respectively. In contrast, analysis of the Sn K-edge extended X-ray absorption fine structure of XAS revealed almost identical values for the Sn-O bond length of SnO film and SnO powder (bulk). These results strongly suggest shrinkage of the interlayer Sn-Sn bond and distortion of the Sn-O pyramid structure in the SnO thin film (Fig. 2), which affects the electronic structure. Our findings demonstrate the importance of direct and precise observation of the electronic characteristics *in thin-film form*, and provide valuable insights into the realization of actual thin-film devices [14].

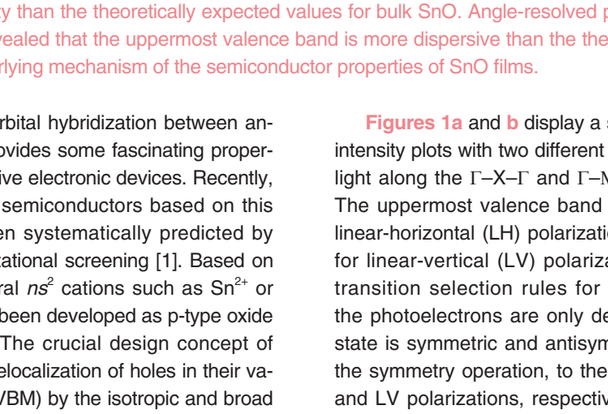

Figure 1: ARPES intensity plots of SnO film along a the Γ–X and b Γ–M lines taken at $h\nu$ = 158 eV with LH and LV polarized light. Calculated band structures (solid lines) were superimposed. Reprinted with permission from Minohara *et al.* [14]. Copyright 2022 *American Chemical Society.*

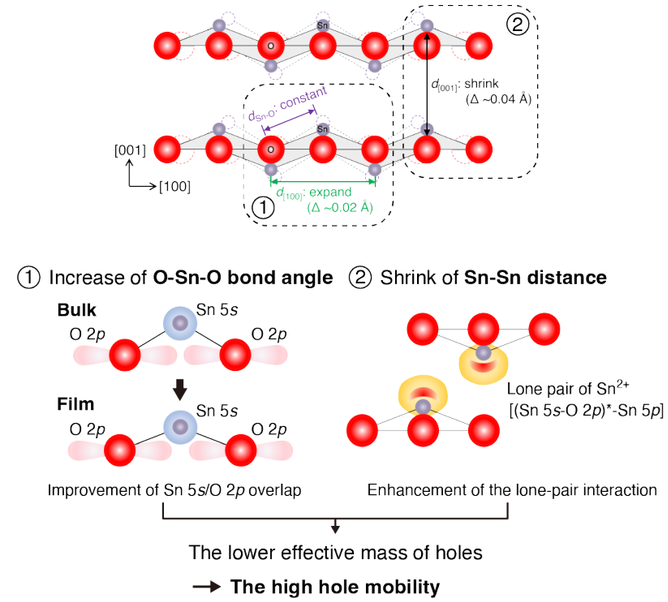

Figure 2: Schematic image of distortion of the Sn-O pyramid structure of SnO film. Broken lines and symbols indicate the original positions in the intralayer Sn-O plane. Adapted with permission from Minohara *et al.* [14]. Copyright 2022 *American Chemical Society.*

REFERENCES

[1] G. Hautier, A. Miglio, G. Ceder, G. -M. Rignanese and X. Gonze, *Nat. Commun.* **4**, 2292 (2013).
[2] A. Bhatia, G. Hautier, T. Nilgianskul, A. Miglio, J. Sun, H. J. Kim, K. H. Kim, S. Chen, G. -M. Rignanese, X. Gonze and J. Suntivich, *Chem. Mater.* **28**, 30 (2016).
[3] N. Kikuchi, A. Samizo, S. Ikeda, Y. Aiura, K. Mibu and K. Nishio, *Phys. Rev. Mater.* **1**, 021601 (2017).
[4] A. Samizo, N. Kikuchi, Y. Aiura, K. Nishio and K. Mibu, *Chem. Mater.* **30**, 8221 (2018).
[5] M. Minohara, Y. Dobashi, N. Kikuchi, A. Samizo, K. Tsukuda, K. Nishio, K. Mibu, K. Kumigashira, I. Hase, Y. Yoshida and Y. Aiura, *Inorg. Chem.* **60**, 8035 (2021).
[6] M. Minohara, N. Kikuchi, K. Tsukuda, Y. Dobashi, A. Samizo, K. Nishio, X. He, T. Katase, T. Kamiya and Y. Aiura, *Mater. Des.* **216**, 110549 (2022).
[7] M. Minohara, A. Samizo, N. Kikuchi, K. K. Bando, Y. Yoshida and Y. Aiura, *J. Phys. Chem. C* **124**, 1755 (2020).
[8] Y. Hu, J. Hwang, Y. Lee, P. Conlin, D. G. Schlom, S. Datta and K. Cho, *J. Appl. Phys.* **126**, 185701 (2019).
[9] S. Hüfner, "*Photoelectron Spectroscopy*"; (Springer-Verlag press, Berlin Heidelberg, 1995).
[10] A. Togo, F. Oba, I. Tanaka and K. Tatsumi, *Phys. Rev. B* **74**, 195128 (2006).
[11] V. -A. Ha, F. Ricci, C. -M. Rignanese and G. Hautier, *J. Mater. Chem. C* **5**, 5772 (2017).
[12] W. Zhou and N. Umezawa, *Phys. Chem. Chem. Phys.* **17**, 17816 (2015).
[13] D. R. Kripalani, P. -P. Sun, P. Lin, M. Xue and K. Zhou, *Phys. Rev. B* **100**, 214112 (2019).
[14] M. Minohara, I. Hase and Y. Aiura, *J. Phys. Chem. Lett.* **13**, 1165 (2022).

BEAMLINES

BL-13B and NW10A

M. Minohara, I. Hase and Y. Aiura (AIST)